Indonesian Physical Review

Volume 09 Issue 02, May 2026

P-ISSN: 2615-1278, E-ISSN: 2614-7904

Structural and Compositional Characterization of Hydroxyapatite and Nano-chitosan Synthesized from *Pinctada maxima* Shell Waste for Biomedical Applications

Susi Rahayu[1,2], D.J.D.H Santjojo[1], Rahadi Wirawan[2], Weny Yulianingsih[2], and Masruroh[1*]

[1]Department of Physics, Faculty of Mathematics and Natural Sciences, Universitas Brawijaya, Malang, 65145, Indonesia

[2]Department of Physics, Faculty of Mathematics and Natural Sciences, University of Mataram, Mataram, 83125, Indonesia

Corresponding Authors E-mail: ruroh@ub.ac.id

Article Info

Article info:

Received: 11-09-2025
Revised: 18-12-2025
Accepted: 13-02-2026

Keywords:

Biomaterials, Biopolymers, Deacetylation degree, Ionic gelation, Sustainable synthesis

How To Cite:

S. Rahayu, D.J.D.H Santjojo, R. Wirawan, W. Yulianingsih, and Masruroh, "Structural and Compositional Characterization of Hydroxyapatite and Nano-chitosan Synthesized from Pinctada maxima Shell Waste for Biomedical Applications", Indonesian Physical Review, vol. 9, no. 2, p 269-285, 2026.

DOI:

https://doi.org/10.29303/ipr.v9i2.574.

Abstract

Pearl oyster (Pinctada maxima) aquaculture in West Nusa Tenggara (NTB), Indonesia, generates underutilized shell waste that may impact coastal environments. This study aimed to convert the Pinctada maxima shell waste into high-value biomaterials, specifically hydroxyapatite (HA) and nano-chitosan, and to characterize their physicochemical properties for potential biomedical applications. HA was synthesized via the wet precipitation method followed by calcination at 1000 °C and 1100 °C. Concurrently, nano-chitosan was prepared through ionic gelation, investigating the effect of 70% and 80% NaOH alkaline treatments. Characterization of HA using EDX indicated a stable Ca/P molar ratio of 1.68 ± 0.03 (1000°C) and 1.67 ± 0.03 (1100°C), FTIR confirmed the presence of hydroxyl and phosphate groups, and XRD revealed well-defined crystalline structures. For nano-chitosan, particle size analysis (PSA) showed size ranges from 235.55 ± 43.90 up to 2728.58 ± 258.74 nm (70% NaOH) and 20.63 ± 18.04 up to 3525.55 ± 13.06 nm (80% NaOH), with FTIR confirming successful ionic cross-linking. The degree of deacetylation (DD) was found to be high, 81.13 ± 0.03% and 82.65 ± 0.15% respectively, although the XRD patterns indicated a predominantly amorphous structure for the nano-chitosan. These findings suggest that the synthesized HA and nano-chitosan from Pinctada maxima shell waste possess favorable physicochemical characteristics, thus supporting their potential as sustainable materials for various biomedical applications.

Introduction

Pearl oyster (*Pinctada maxima*) farming is one of the leading non-mining export commodities in West Nusa Tenggara (NTB), Indonesia. The NTB Department of Trade reported that export

data indicated a total of 670 kg of pearls exported in 2022, making it a major contributor to Indonesia's sea pearl production. This pearl farming generates a substantial amount of biomass waste in the form of oyster shells. To date, pearl oyster shell waste in NTB has not been fully utilized, with most being discarded, potentially causing environmental issues in coastal areas. In fact, pearl oyster shells can serve as a valuable source of calcium carbonate ($CaCO_3$) for the production of hydroxyapatite (HA) and chitin. *Pinctada maxima* shells contain a high $CaCO_3$ content (up to 99%), supporting both the utilization of waste and the sustainable use of marine resources [1].

Hydroxyapatite ($Ca_{10}(PO_4)_6(OH)_2$) is a bioceramic material that closely resembles the mineral components of human bone and teeth. Recent studies have shown that HA possesses high bioactivity, biocompatibility, and osteoconductivity, making it suitable for applications in bone grafts, dental implants, and scaffolds [2][3]. The wet precipitation method is widely used to synthesize hydroxyapatite due to its simplicity and cost efficiency. In addition, this method allows control of crystal morphology by adjusting reaction variables such as pH, calcination temperature, precursor ratio, and calcination duration. Recent studies show that alkaline precipitation (pH 9–11) increases the dissolution of calcium ions from shell-derived sources and suppresses the secondary phase, resulting in high-quality hydroxyapatite with an optimal Ca/P ratio (~1.67) [3]. Calcination temperature also plays a crucial role in improving crystallinity, reducing micro strain, and eliminating carbonate impurities. Several studies have demonstrated that heat treatment at high temperatures between 1000 °C and 1200 °C effectively increases crystallinity, removes organic contaminants, enhances density and microhardness, and promotes the formation of bone-like apatite in simulated body fluid tests [4][5].

In addition to HA, nano-chitosan is a polymer-based material that also plays an important role in biomedical activity. Nano chitosan is produced from chitin isolated from shell waste, which is then processed through alkaline deacetylation to achieve a degree of deacetylation exceeding 75%. The ionic gelation method is one of the most commonly used techniques, in which sodium tripolyphosphate (TPP) is employed to produce nanoparticles with sizes below 200 nm. This approach is solvent-free, scalable, and allows precise control over particle size and stability [6]. Although many studies use Natrium Hydroxyde (NaOH) concentrations between 60% and 80% during the deacetylation stage, several reports mainly focus on conventional chitosan isolation without further nano particle synthesis [7][8]. An integrated synthesis approach was demonstrated by Alawiyah et al. (2024), who synthesized nano-chitosan from *Pinctada maxima* shell waste using 80% NaOH. Their process produced a high degree of deacetylation (88.63%) and a zeta potential of -21.6 mV, indicating good colloidal stability. However, the average particle size remained at 2336 nm, suggesting that further optimization is required to achieve the ideal nanoscale range necessary for biomedical applications [9].

Hydroxyapatite (HA) and nano chitosan have been extensively studied as candidate materials for biomedical applications due to their favorable physicochemical properties. According to ISO 13779-3 (2018), HA used in medical implants should possess a minimum phase purity of 95%, high crystallinity, and a Ca/P ratio close to the ideal value of 1.67. These properties enable chemical and structural compatibility with the mineral phase found in natural bone. Such materials must also be free from heavy metal pollutants, such as lead (Pb) and cadmium (Cd), as well as organic contaminants, which could impair their function within the body [10]. Nano-chitosan is considered suitable for biomedical applications if it has a degree of

deacetylation greater than 75%, which enhances antibacterial activity, bio functionality, and colloidal stability. In addition, the particle size should be maintained below 200 nm to allow injectable formulations or integration into regenerative systems [11]. Materials derived from *Pinctada maxima* shell waste can be considered to meet the following criteria: phase purity, optimal Ca/P ratio, high degree of deacetylation, controlled nanoscale particle size, and validated biocompatibility. Although many studies have examined the synthesis of hydroxyapatite and the extraction of chitosan nano particles via ionic gelation methods, very few have explicitly integrated and compared the properties of pure HA from *Pinctada maxima* shells at calcination temperatures of 1000 °C and 1100 °C. Therefore, a more focused investigation is required. Similarly, studies on chitosan nanoparticle extraction via ionic gelation rarely attempt to integrate both extractions from *Pinctada maxima* shells while fully characterizing the resulting bio ceramic and biopolymer components [3]. Comprehensive physicochemical analyses were performed using Energy Dispersive X-ray (EDX), Fourier Transform Infra-Red (FTIR), X-ray Diffraction (XRD), and Particle Size Analyzer (PSA).

Studies on HA and nano chitosan are very interesting because both have the potential to complement each other in the development of hybrid biomaterials. HA can function as an inorganic component with osteoconductive properties, while nano chitosan acts as an organic matrix that enhances bioactivity. Although the synthesis of HA from biogenic sources has been widely reported, most studies still focus on analyzing physicochemical parameters separately. Quantitative analysis that systematically correlates the Ca/P ratio, crystallinity, and density of biogenic hydroxyapatite is still relatively limited. Therefore, this study aims to fill this gap by presenting an integrated physicochemical interpretation of hydroxyapatite synthesized from *Pinctada maxima* shells. In addition, in the chitosan deacetylation process, the use of NaOH concentrations below 50% is more commonly reported, while comparative studies evaluating high NaOH concentrations, such as 70% and 80%, are still limited. In this study, variations in alkali concentration were applied to examine their effect on the degree of deacetylation and the physicochemical characteristics of nano-chitosan, which are important parameters in determining the performance of materials for biomedical applications. The physicochemical characteristics obtained from this study are expected to provide initial insights as a fundamental basis for the development of hybrid materials in the future, as well as enrich the understanding of the synthesis and characterization strategies of HA and nano-chitosan based on *Pinctada maxima* shells.

Experimental Method

Tools and Material

The primary biomaterial was pearl oyster shell (*Pinctada maxima*), collected from the coastal waters of West Nusa Tenggara, Indonesia. All reagents utilized were of pro-analyst grade. These included acetic acid (CH_3COOH, Mallinckrodt, USA), phosphoric acid (H_3PO_4, UNIVAR, Australia), hydrochloric acid (HCl, Mallinckrodt, USA), ammonium hydroxide (NH_4OH, 25%, Merck, Germany), natrium hydroxide (NaOH, Merck, Germany), sodium tripolyphosphate (TPP, 0.1%, Xilong Scientific, China), and Tween 80 (0.1%, Sigma Aldrich, Germany).

The equipment employed for sample preparation and processing consisted of a 100-mesh stainless steel sieve (KZM, Indonesia), an electric blender, petri dishes, glass funnels, beakers, graduated cylinders, glass stirring rods, and a mortar and pestle. Milling and grinding were performed using a miller machine (FCT-100, Fomac, Indonesia) and a pulp grinder (SY-150,

Yamamoto, Indonesia), respectively. Additional instruments included a digital analytical balance, oven (Mito, Indonesia), volumetric pipettes, magnetic stirrer with integrated hot plate (IKA C-MAG HS7, Indonesia), magnetic stirring bars, Whatman No. 42 filter paper (Whatman, UK), pH indicator strips (Merck, Germany), droppers, and a manual stopwatch.

Research Procedures

Preparation of Calcium Carbonate Powder

The initial step involved cleaning the *Pinctada maxima* shells to remove surface impurities. Both the inner and outer surfaces of the shells were scrubbed thoroughly using distilled water and 86% ethanol. The cleaned shells were then immersed in distilled water for 24 hours to eliminate residual organic matter. After soaking, the shells were dried at 70 °C for 2 hours. In the second stage, the dried shells were crushed using a mechanical grinder, followed by further milling with a high-speed miller to obtain fine calcium carbonate ($CaCO_3$) powder. The obtained powder was sieved through a 100-mesh stainless steel sieve to ensure even particle size distribution.

Synthesis of Hydroxyapatite

Hydroxyapatite was synthesized via a wet precipitation method, adapted with modifications from the procedure reported by Ng et al. (2022) (Figure 1) [12]. The modifications were at the final stage of synthesis where, in this study the final process was to calcinate the samples using temperature variations. Initially, calcium carbonate ($CaCO_3$) powder derived from *Pinctada maxima* shells was subjected to calcination at 1100 °C for 6 hours in a muffle furnace. During calcination, $CaCO_3$ was thermally decomposed into calcium oxide (CaO), releasing carbon dioxide (CO_2) as a by-product, as described by Sangmala et al. (2021) [13]. Subsequently, 5.6 g of CaO powder was dissolved in 200 mL of distilled water and titrated with 200 mL of 0.3 M phosphoric acid (H_3PO_4) at a rate of 15 mL/minute at a speed of 600 rpm under continuous stirring using a magnetic stirrer. The pH was maintained at approximately 10 by adding Ammonium Hydroxide solution (NH_4OH, Merck, Germany). The suspension was further stirred at 80 °C for 1 hour to promote precipitation. After stirring, the mixture was aged at room temperature for 24 hours to allow complete precipitation. The milky-white precipitate was recovered by filtration and dried at 100°C for 4 hours. The overall reaction involved in HA production is described as follows:

$$CaO + H_2O \longrightarrow Ca(OH)_2 \quad (1)$$

$$10Ca(OH)_2 + 6H_3PO_4 \longrightarrow Ca_{10}(PO_4)_6(OH)_2 + 18H_2O \quad (2)$$

The dried precipitate was finely pulverized with a mortar and pestle to produce a homogeneous powder. Thermal calcination of the powder at 1000 °C and 1100 °C for 3 hours improved crystallinity and eliminated organic components. The samples were cooled naturally to room temperature inside the furnace. The resultant hydroxyapatite was then analyzed by using EDX Spectroscopy, FTIR, and XRD to determine elemental composition, functional groups, and evaluate phase composition and crystallinity, respectively.

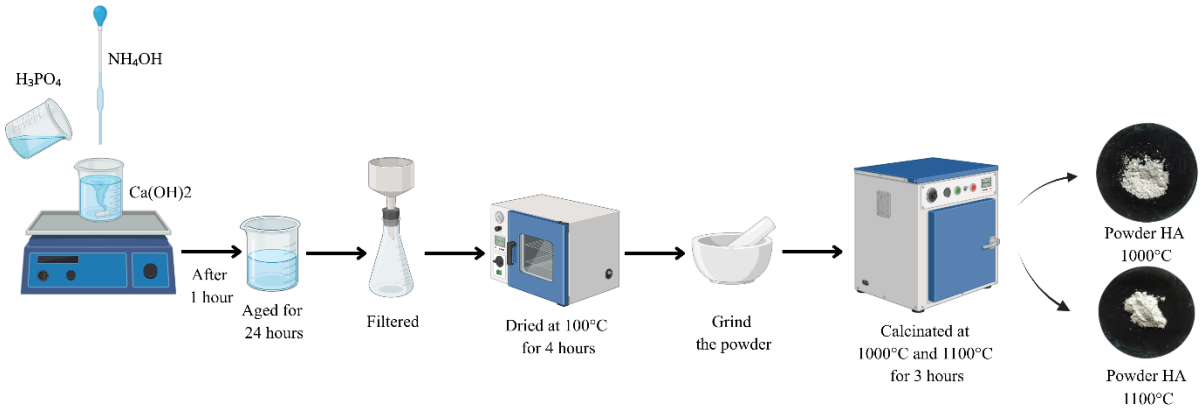

Figure 1. Hydroxyapatite synthesis process from *Pinctada maxima* shells

Synthesis of Nano chitosan

Nano chitosan was extracted following the procedures described by Nurmaulida et al. (2023) and Alawiyah et al. (2024), although with a few changes [1][9]. Previous research used 60% Natrium Hydroxide (NaOH) during the deacetylation stage; in this study, NaOH concentrations of 70% and 80% were employed to examine their effects on the properties of chitosan. The total extraction process was divided into four steps (Figure 2): deproteinization, demineralization, deacetylation, and ionic gelation. To deproteinize, 80 g of finely crushed *Pinctada maxima* powder was mixed in 800 mL of 4% NaOH solution and stirred at 80 °C for an hour. The suspension was then washed to reach neutral pH, and the residue was dried at 80°C for 3 hours. The dried material was subjected to demineralization by adding it in 1 M hydrochloric acid (HCl) (1:15 (w/v)) for 1 hour under continuous stirring. The resulting slurry was neutralized through repeated washing, followed by drying at 80 °C for 3 hours. The deacetylation step aimed to convert acetyl groups into amino groups, producing chitosan. The chitin powder was reacted with NaOH solution (1:15 (w/v)) at 120 °C for 3 hours. The resulting precipitate was then washed and dried at 60 °C for 5 hours.

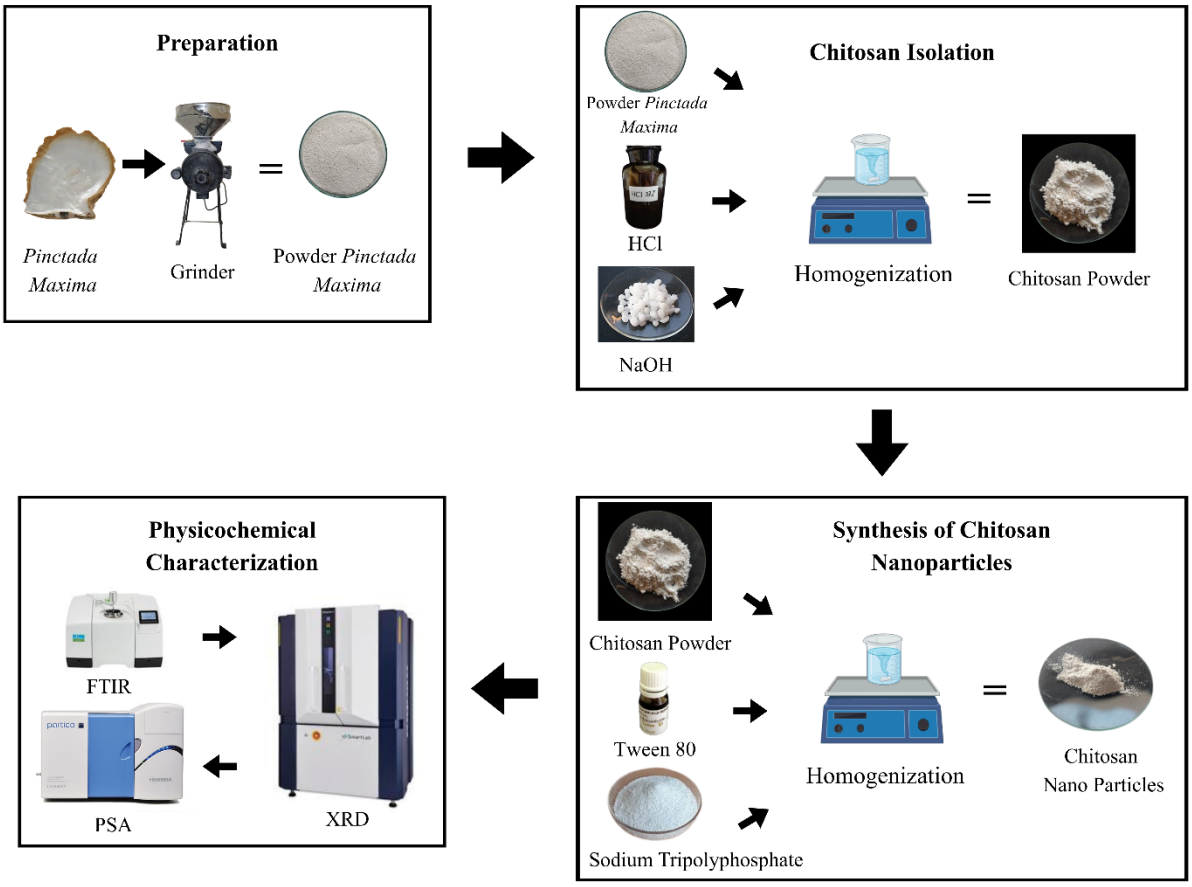

Figure 2. The schematic illustration synthesis of nano chitosan from *Pinctada maxima* shells

Subsequently, chitosan powder was converted into nano chitosan using the ionic gelation technique as described by Patel & Jain (2024), with slight modifications [6]. Briefly, 3 g of chitosan was dissolved in 60 mL of 1% acetic acid solution (v/v) and then diluted with 1 L of deionized water. The mixture was homogenized at 1000 rpm for 90 minutes. Following this, 25 mL of 0.1% (v/v) Tween 80 was added gradually while maintaining stirring at 1000 rpm for an additional 60 minutes. Once the solution was fully homogenized, 200 mL of 0.1% (w/v) sodium tripolyphosphate (TPP) was slowly introduced into the chitosan solution under constant stirring at 1000 rpm for 120 minutes to facilitate ionic cross-linking. The pH was adjusted using deionized water to reach neutrality. The final suspension was then subjected to drying at 50 °C for 5 hours to obtain nano chitosan powder. The physicochemical properties of nano-chitosan were analyzed using FTIR, XRD, and Particle Size Analyzer (PSA).

Data analysis

The synthesized hydroxyapatite (HA) was subjected to physicochemical characterization, including the Ca/P molar ratio, functional groups, crystallinity, crystallite size, and crystal structure. Functional group analysis was performed using Fourier Transform Infrared (FTIR), with characteristic absorption bands corresponding to the functional groups of hydroxyapatites, specifically hydroxyl (OH^-), phosphate (PO_4^{3-}), and carbonate (CO_3^{2-}) groups.

In the case of nano chitosan, functional groups such as amine (NH) and hydroxyl (OH) were also confirmed by using FTIR. Crystal structure was conducted using X-ray Diffraction (XRD), providing both qualitative and quantitative data, where the degree of crystallinity was determined using the following Equation (3) [14]:

$$\text{Crystallinity} = \frac{\text{Area Fraction Crystalline}}{\text{Area Fraction Crystalline +Amorphous}} \times 100\% \quad (3)$$

In addition, the crystallite size of hydroxyapatite was determined using the Debye–Scherrer equation, as follows:

$$\text{D} = \frac{K\lambda}{\beta \cos \theta} \quad (4)$$

where D is the crystallite size (nm), K is the shape factor (0.89), λ is the wavelength of the X-ray (1.5406 Å), β is the full width at half maximum (FWHM) (radians), and θ is the Bragg diffraction angle (in degrees).

The synthesized nano chitosan was further analyzed for its physicochemical properties, including organoleptic characteristics, yield, degree of deacetylation (DD), functional groups, qualitative and quantitative crystal structure, and particle size. Organoleptic parameters such as color, odor, and morphology were evaluated using human sensory observation. The yield of nano chitosan was calculated based on the ratio between the initial mass of the pearl oyster shell powder (m_0) and the final mass of the resulting nano chitosan (m_t), following Equation (5) [15]:

$$\text{Yield (\%)} = \frac{m_t}{m_o} \times 100\% \quad (5)$$

The degree of deacetylation of chitosan, along with the functional groups, was identified based on FTIR spectral data. The degree of deacetylation was determined by calculating the absorbance ratio between the amine group (NH_2) and the hydroxyl group (OH), which was calculated using Equations (6) [16]:

$$\text{DD (\%)} = \left[100 - \left(\frac{A_{1655}}{A_{3450}} \times \frac{100}{1.33}\right)\right] \quad (6)$$

The degree of deacetylation (DD) is expressed as a percentage and represents the proportion of acetyl groups removed and calculated based on absorbance values from FTIR spectrum, where A indicates absorbance, A_{1655} and A_{3450} are the absorbance at the amide I band (1655 cm^{-1}) and at the hydroxyl group (3450 cm^{-1}), respectively.

In addition to FTIR analysis, the physicochemical properties of nano-chitosan were investigated using XRD to determine the qualitative and quantitative aspects of its crystalline structure. XRD analysis was conducted over a 2θ range of 10° to 80° and λ = 1.5406 Å. The crystallinity and phase identification were determined by comparing diffraction patterns to standard reference data. The Scherrer equation was employed to calculate the average

crystallite size, where the degree of crystallinity was determined by comparing the crystalline peak areas to the total diffractogram area. Furthermore, particle size distribution was examined using PSA, which has a substantial impact on the physical properties and performance of the final product. The PSA additionally provided the polydispersity index (PDI), which measures the homogeneity of particle sizes in the samples.

Result and Discussion

Hydroxyapatite

Hydroxyapatite (HA) has been effectively synthesized from *Pinctada maxima* pearl oyster shell waste. The purity of the resultant substance was confirmed via elemental composition analysis with EDX. The EDX results revealed a predominant presence of calcium (Ca), phosphorus (P), and oxygen (O) (Figure 3), which was consistent with the theoretical stoichiometry of HA and confirmed the success of the synthesis process. The comparatively high oxygen content can be attributed to two main sources. Firstly, hydroxyl groups (OH^-) are an integral component of HA's crystal structure, inherently contributing to the oxygen signal. Secondly, the hydrophilic surface of HA has a propensity to adsorb moisture from the surrounding environment during sample preparation, which may elevate the oxygen reading [17].

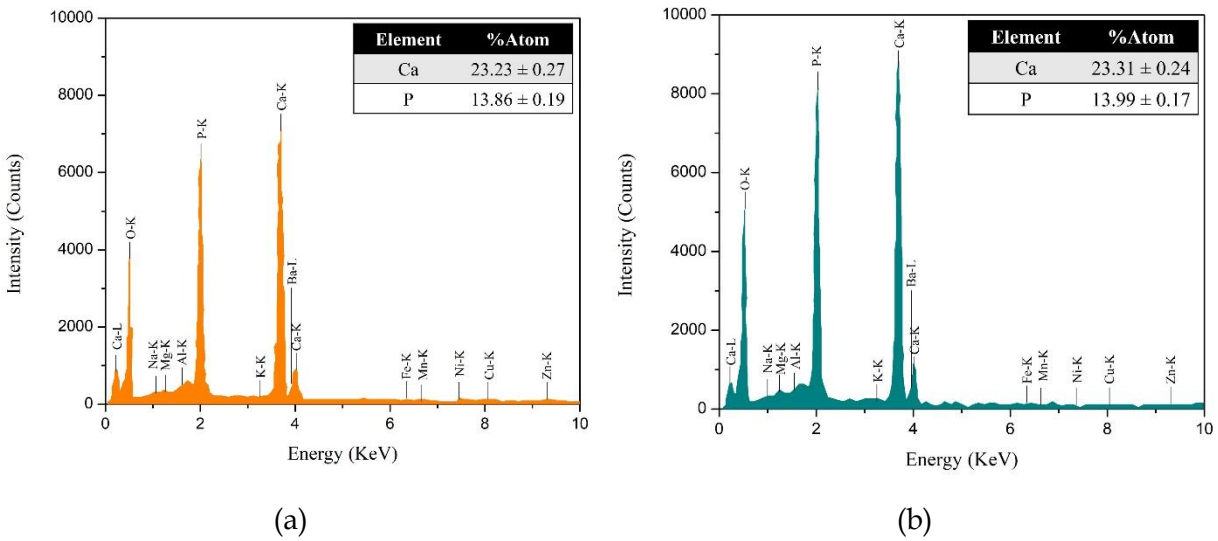

(a) (b)

Figure 3. Analysis of constituent elements with different calcination temperature parameters (a) 1000 ℃ and (b) 1100 ℃

Additionally, minor elemental traces were detected post-sintering; however, their concentrations were negligible and did not significantly affect the final composition or structural integrity of the HA (Table 1). Overall, the elemental profile obtained through EDX strongly supports the high purity of the synthesized HA, indicating its suitability for biomedical applications.

Complementing the elemental data, the Ca/P molar ratio serves as a critical parameter in evaluating the structural fidelity of HA. Pure HA typically exhibits Ca/P = 1.67, closely resembling the mineral composition of natural bone and dental tissue [18]. In this study, the HA obtained showed a Ca/P ratio of 1.68 ± 0.03 at 1000°C and exactly 1.67 ± 0.03 at 1100°C (Table 1). The calculations were performed with three repetitions, and the results showed that both samples were close to the ideal stoichiometric ratio of pure HA. Compared with the Ca/P ratio in previous studies synthesized from the same source, namely *Pinctada maxima*, where a Ca/P ratio of 1.72 – 2.15 was obtained [19][20][21]. This conformity further validates the successful synthesis and compositional integrity of the material for potential biomedical use.

Table 1. Elemental composition of hydroxyapatite samples at different calcination temperatures based on EDX analysis

Elements	Percentage of Minerals (%)	
	1000 °C	1100 °C
O	61.13 ± 1.19	62.08 ± 1.07
Na	0.20 ± 0.04	0.17 ± 0.04
Mg	0.23 ± 0.03	0.26 ± 0.03
Al	0.07 ± 0.02	0.06 ± 0.02
P	13.86 ± 0.19	13.99 ± 0.17
K	0.04 ± 0.02	0.03 ± 0.01
Ca	23.23 ± 0.27	23.31 ± 0.24
Mn	0.02 ± 0.02	-
Fe	-	0.04 ± 0.02
Ni	0.04 ± 0.03	-
Cu	1.06 ± 0.12	-
Zn	0.11 ± 0.06	0.06 ± 0.04
Ba	-	-
Total (%)	100.0	100.0

FTIR spectroscopy was employed to further confirm the structural identity of the synthesized HA (Figure 4). Spectral data were recorded at wavenumber of 400 to 4000 cm^{-1} and revealed absorption bands corresponding to key functional groups characteristic of HA, including hydroxyl (OH^-), carbonate (CO_3^{2-}), and phosphate (PO_4^{3-}) moieties [22]. The OH^- functional group appeared prominently at approximately 3560 cm^{-1} and 630 cm^{-1}, indicating that hydroxyl groups were retained in the crystal lattice, even after thermal processing. However, the sample sintered at 1100 °C displayed a noticeable decrease in OH^- peak intensity compared to the sample treated at 1000 °C, suggesting partial dehydroxylation at elevated temperatures. Phosphate group vibrations were also distinctly identified between 500 and 1100 cm^{-1}, particularly at 563 cm^{-1}, 603 cm^{-1}, and 1030 cm^{-1}. Minor shifts in peak positions and variations in transmittance between the two samples suggest improved atomic and molecular ordering, likely resulting from increased crystallinity during sintering.

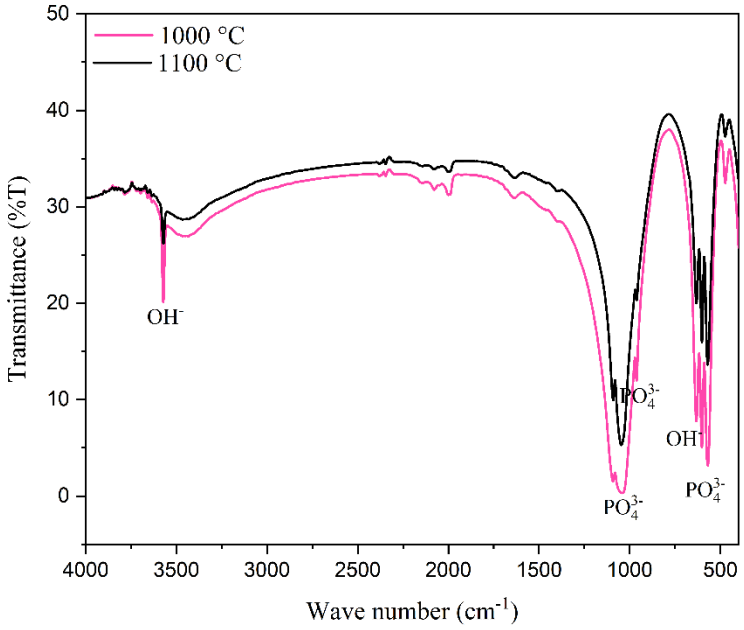

Figure 4. FTIR spectra of hydroxyapatite synthesized at 1000 °C and 1100 °C

The FTIR findings were corroborated by X-ray diffraction (XRD) analysis, which provided quantitative evidence of the material's crystallinity and phase structure. The XRD diffraction patterns (Figure 5) indicated that both samples, sintered at 1000 °C and 1100 °C, exhibited a predominantly hexagonal crystal structure, consistent with *Joint Committee on Powder Diffraction Standards* (JCPDS) No. 09-0432 for hydroxyapatite (HA). Additionally, a minor β-tricalcium phosphate (β-TCP) phase was identified (JCPDS No. 09-0169), which commonly emerges due to calcium-phosphate imbalance at elevated temperatures. The presence of β-TCP in the material is not merely considered an impurity, but can provide functional contributions for biomedical applications. Several studies have reported that β-TCP exhibits greater biodegradability and resorbability in biological environments compared to HA, thereby potentially accelerating bone regeneration processes [23]. Meanwhile, the more stable HA plays a role in maintaining long-term structural stability. The combination of both phases produces a synergistic effect, balancing mechanical stability and bioresorbability. Therefore, although this study primarily targets the synthesis of HA, the presence of a minor β-TCP phase may broaden the potential applicability of the material, as it indicates opportunities for developing calcium phosphate-based biomaterials with enhanced bioactivity. The degree of crystallinity increased from 67.79 ± 6.44% at 1000 °C to 69.17 ± 7.66% at 1100 °C, aligning with the sharpening of diffraction peaks that reflect enhanced atomic ordering within the crystal lattice. These findings further support the FTIR results, suggesting that higher sintering temperatures enhance the molecular and atomic order of the material.

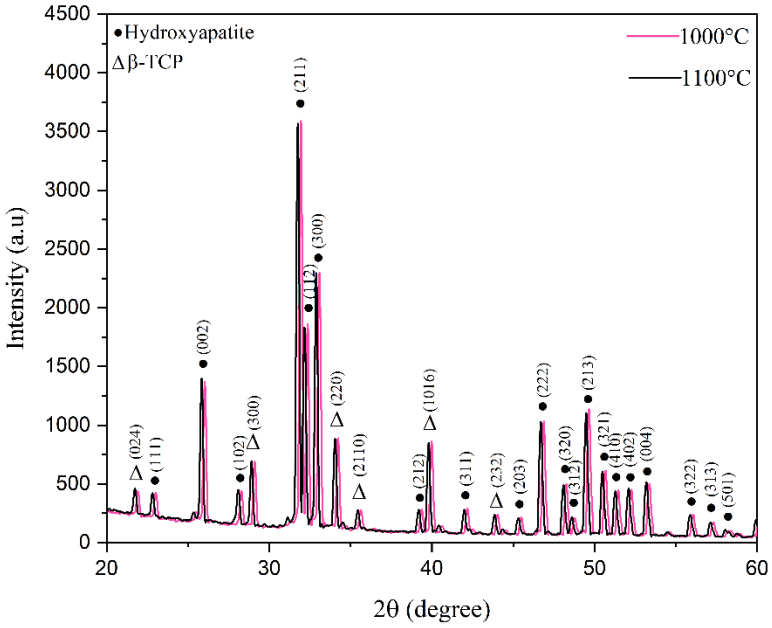

Figure 5. XRD patterns of hydroxyapatite synthesized at 1000 °C and 1100 °C

The increase in crystallinity was also reflected in the change in crystal density, which decreased from 2747 kg/m³ at 1000 °C to 2786 kg/m³ at 1100 °C, indicating lattice restructuring at higher sintering temperatures. The FTIR and XRD results show that hydroxyapatite made from *Pinctada maxima* shell waste has the correct chemical composition and crystal structure. This makes it suitable for biomedical applications.

Nano-chitosan

Nano-chitosan was successfully synthesized through four main stages: deproteinization, demineralization, deacetylation, and ionic gelation. This process yielded a final product in the form of a cream-colored, odorless powder. In addition to organoleptic evaluation, the samples were also analyzed to determine the yield obtained from the overall isolation process up to the production of nano chitosan (Table 2). Based on Table 2, the final mass of the two samples showed a notable difference: the sample treated with 70% NaOH yielded 3.15 ± 0.05 %, while the 80% NaOH sample yielded only 2.27 ± 0.84 %. This reduction in mass correlates with the higher NaOH concentration, which tends to decrease yield due to greater loss of material during the isolation and nano-chitosan synthesis processes. This finding is consistent with previous studies reporting that higher NaOH concentrations accelerate deacetylation but may also lead to reduced product yield, as parts of the natural polymer structure are degraded or lost during washing steps [24]. In general, the mass reduction reflects the chemical reaction mechanisms and material recovery efficiency at each step of the isolation process.

Table 2. Yield data for each stage of nano chitosan isolation

Sample	Process	Initial mass (m_0) (gram)	Final mass (m_t) (gram)	Yield (%)
NaOH 70%	Deproteination	80.00 ± 0.00	77.71 ± 0.26	97.14 ± 0.32
	Demineralization	77.71 ± 0.26	25.35 ± 4.62	32.63 ± 6.00
	Deacetylation	25.35 ± 4.62	3.01 ± 0.54	11.92 ± 0.95
	Nano-chitosan	80.00 ± 0.00	2.52 ± 0.04	3.15 ± 0.05
NaOH 80%	Deproteination	80.00 ± 0.00	76.85 ± 1.28	96.06 ± 1.60
	Demineralization	76.85 ± 1.28	28.00 ± 0.32	36.45 ± 0.71
	Deacetylation	28.00 ± 0.32	2.05 ± 0.15	7.33 ± 0.20
	Nano-chitosan	80.00 ± 0.00	1.82 ± 0.67	2.27 ± 0.84

The synthesized powder derived from pearl oyster shells was identified as chitosan material based on FTIR spectroscopy analysis (Figure 6). This identification was supported by the appearance of absorption bands corresponding to characteristic functional groups of nano-chitosan, specifically secondary amine (–NH) and hydroxyl (–OH) groups, in both analyzed samples.

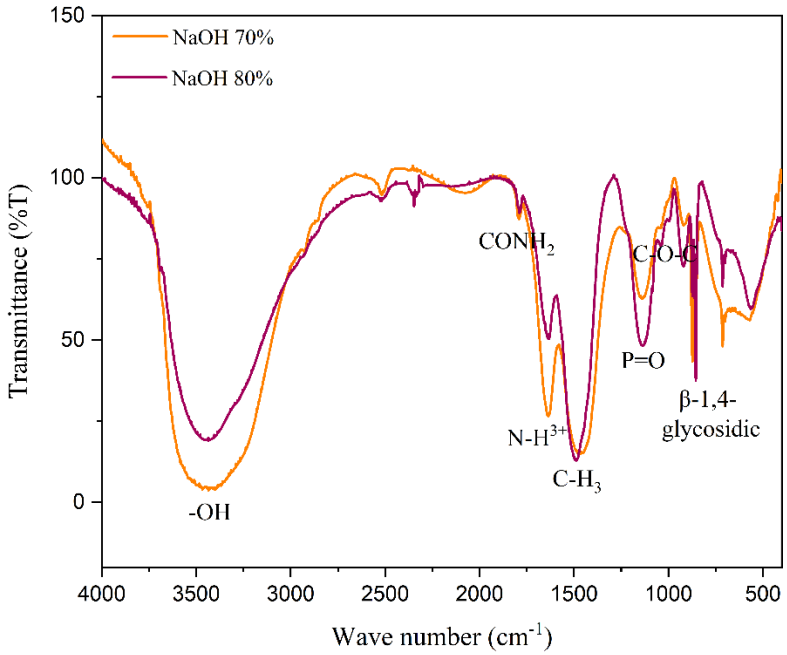

Figure 6. FTIR spectra of nano-chitosan samples synthesized using 70% and 80% NaOH

Both nano-chitosan samples exhibited relatively similar infrared spectra, although slight differences were observed. These variations are most likely due to differences in the isolation processes, which can affect the wavenumber positions of the –OH and –NH absorption bands [8]. The observed shifts in wavenumber for these bands are attributed to ionic interactions between the ammonium groups ($-NH_3^+$) on the chitosan chains and the phosphate groups (PO_4^{3-}) from sodium tripolyphosphate (TPP), which acted as the crosslinking agent. This interaction causes a shift towards lower wave numbers, indicating a change in the vibrational

energy of the bond due to the formation of ionic bonds. The amide groups (–$CONH_2$) present in the chitosan structure also contributed to the spectral profile, particularly in the amide I (C=O stretching) and amide II (N–H bending) regions. Additionally, the presence of distinct phosphate absorption bands at 1250–900 cm^{-1} corresponds to P=O stretching and P–O–P bending, which confirms the successful formation of chitosan–phosphate complexes via the ionic gelation process. This confirms that the isolation and crosslinking procedures effectively produced nano-chitosan with the desired chemical characteristics.

The purity of the synthesized nano-chitosan was further confirmed by calculating the degree of deacetylation (DD) (Eq. 6). DD reflects the extent of chitin-to-chitosan conversion via acetyl group removal, where a higher DD value indicates better quality and purity [7]. Based on the analysis, the sample treated with 70% NaOH exhibited a DD of 81.13 ± 0.03%, while the sample processed with 80% NaOH showed a higher DD of 82.65 ± 0.15%. This increase in DD was directly correlated with the stronger alkaline conditions used during the deacetylation process [25]. Both DD values met the minimum purity requirements established by the Indonesian National Standard (BSN), the European Pharmacopoeia 6.0 (Eur. Ph 6.0), and the United States Pharmacopeia 34-NF 29 (USP 34-NF 29). These results indicate that the resulting nano-chitosan has properties suitable for potential applications in the food and healthcare sectors.

The particle size characteristics of nano-chitosan were analyzed using a Particle Size Analyzer (PSA) as an important parameter in nanoparticle classification. The measurement results showed differences in particle size distribution between the two samples (Table 3). The D10 values of both samples were within the nanoparticle range, namely 235.55 ± 43.90 nm for the 70% NaOH treatment and 20.63 ± 18.04 nm for the 80% NaOH treatment, indicating the formation of nano-chitosan fractions. However, the D50 and D90 values were still within the micrometer range, ranging from 2265.00 ± 147.36 nm to 2728.58 ± 258.74 nm (70% NaOH) and 2121.82 ± 1832.75 nm to 3525.55 ± 13.06 nm (80% NaOH), respectively. This indicates particle aggregation, which is likely caused by strong intermolecular hydrogen bonds and the tendency of particles to clump together after the drying process.

Table 3. Particle size distribution using particle size analyzer

Sample	D10 (nm)	D50 (nm)	D90 (nm)	Mean (nm)
NaOH 70%	235.55 ± 43.90	2265.00 ± 147.36	2728.58 ± 258.74	2101.83 ± 9 1.61
NaOH 80 %	20.63 ± 18.04	2121.82 ±1832.75	3525.55 ± 13.06	2491.10 ± 927.37

Although the nanometer fraction is not dominant, the results of the study show that the deacetylation process using 70 – 80 % NaOH is capable of producing nano-sized components and affecting the stability of particle dispersion. This observation is consistent with previous studies, such as the research by Gamboa et al. (2024), which reported particle sizes ranging from 51 to 195 nm when adjusting the chitosan-to-TPP ratio [26]. Their findings highlight that synthesis parameters, including the alkali concentration used during deacetylation, have a significant impact on the final morphology of nano chitosan. A similar observation was made in this study, where higher NaOH concentrations resulted in smaller and more uniform nano-sized fractions, supporting the relationship between deacetylation conditions and particle characteristics.

Particles smaller than 200 nm are suitable for biomedical applications such as scaffolds, wound healing, and drug delivery. At this size range, particles are able to penetrate cell membranes, enhance biological distribution, and maintain colloidal stability in physiological environments [27]. Therefore, despite the presence of agglomerated particles, nano-chitosan synthesized from *Pinctada maxima* shell waste still exhibits characteristics that make it a promising candidate for biomedical use. Additional optimization, including ultrasonication, the addition of stabilizing agents, or more controlled precipitation methods, can help achieve a narrower and more uniform particle size distribution, suitable for biomedical applications.

Another essential characteristic for achieving medical-grade standards in nano-chitosan is its crystallinity, which may be determined by XRD analysis (Figure 7). This approach identifies the materials structural order, which is critical in defining its physical qualities, stability, and biological performance in biomedical applications.

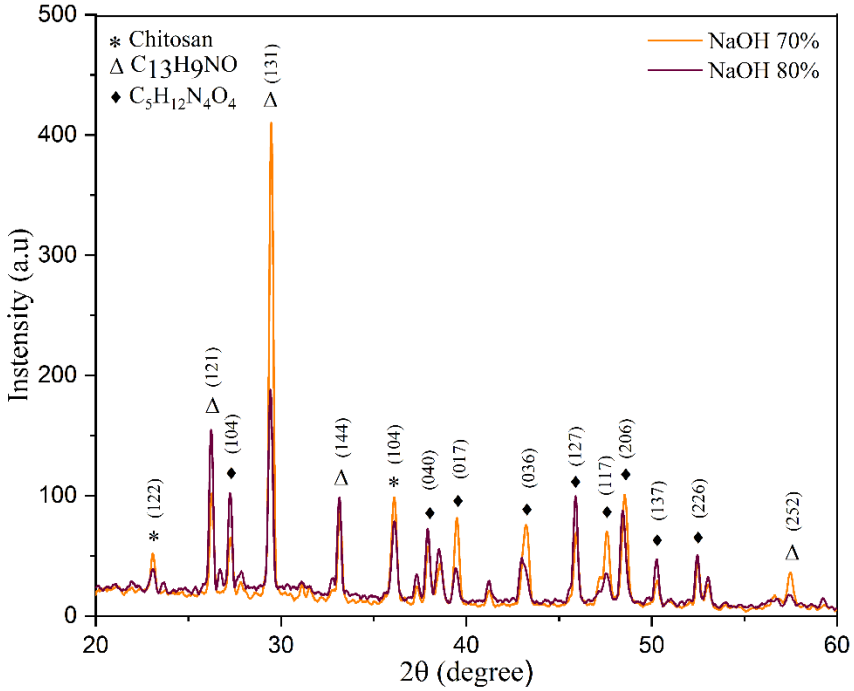

Figure 7. XRD pattern of nano-chitosan particles synthesized from *Pinctada maxima*

Based on the XRD pattern, both nano-chitosan samples showed a structure dominated by the amorphous phase, characterized by broad diffraction peaks and low intensity. This characteristic is consistent with the basic nature of chitosan, a natural polymer with long molecular chains and active functional groups (Figure 6). These properties result in low structural regularity and prevent the formation of well-defined crystal lattices. Based on JCPDS No. 39-1894, chitosan generally exhibits diffraction signals in the 2θ range of 13.6°–37.9° , but in both samples, these peaks appear very broad, indicating a low degree of crystallinity. Quantitatively, the sample processed using 70% NaOH had a degree of

crystallinity of 4.70 ± 0.31% with a crystal density of 2193 kg/m³, while the 80% NaOH sample showed a slightly lower degree of crystallinity of 4.32 ± 0.08% but with an increase in crystal density to 2453 kg/m³. This dominant amorphous property is actually beneficial for biomedical applications because it can increase the solubility, bioavailability, and biological interaction ability of nano-chitosan [27][28]. Both samples adopted an orthorhombic structure. These observations suggest that, despite low crystallinity, the increase in crystal density with higher NaOH concentration may be attributed to tighter molecular packing and increased crosslinking interactions with tripolyphosphate (TPP) during ionic gelation. The amorphous nature of nano-chitosan is commonly associated with the disruption of crystalline domains by TPP counterions, which penetrate the polymer matrix and hinder lattice formation. This phenomenon, frequently reported in chitosan nanoparticles synthesized via ionic gelation, contributes positively to biomedical performance by enhancing solubility, swelling behavior and bio interaction potential [29].

Conclusion

Hydroxyapatite (HA) and nano-chitosan were synthesized from *Pinctada maxima* shell waste using wet precipitation and ionic gelation methods. The synthesized HA exhibited an ideal Ca/P ratio of 1.68 ± 0.03 (1000°C) and 1.67 ± 0.03 (1100°C) and characteristic FTIR bands corresponding to hydroxyl and phosphate groups, with increased crystallinity observed at higher calcination temperatures. The presence of β-TCP as a secondary phase was also identified, likely influenced by synthesis conditions and thermal parameters. Nano-chitosan obtained via ionic gelation following alkaline deacetylation achieved high degrees of deacetylation (81.13 ± 0.03% and 82.65 ± 0.15%.) and exhibited characteristic –OH and –NH functional groups as confirmed by FTIR. PSA analysis shows that particles formed at a concentration of 80% NaOH are in the range of 235.55 ± 43.90 to 2728.58 ± 258.74 nm (70% NaOH) and 20.63 ± 18.04 to 3525.55 ± 13.06 nm (80% NaOH), with FTIR confirming ionic cross-linking and a degree of deacetylation of 81.13 ± 0.03% and 82.65 ± 0.15%. Although the XRD pattern shows the typical amorphous characteristics of chitin-based polymers, this morphology can be useful for applications that require high surface area and structural flexibility. The physicochemical properties obtained indicate that hydroxyapatite produced from *Pinctada maxima* shell waste has characteristics that are relevant for material development from a sustainability perspective. Meanwhile, nano-chitosan requires further optimization, such as ultrasonication, the addition of stabilizing agents, to achieve a narrower and more uniform particle size distribution, as well as the need to analyze the zeta potential to determine particle stability. Both materials require additional biological evaluation to assess their biocompatibility before biomedical applications can be considered.

Acknowledgment

This research was financially supported by the Ministry of Research and Technology (Kemenristek) through the 2025 Postgraduate Research Scheme, Doctoral Dissertation Research sub-scheme Number: 00606/UN10.A0501/B/PT.01.03.2/2025. The authors gratefully acknowledge this funding support, which enabled the successful completion of this study.

References

[1] S. E. Nurmaulida *Et Al.*, "Fabrication Of Chitosan Biopolymer From Pearl Oyster Shells (*Pinctada Maxima*) For Medical Applications," *Indones. Phys. Rev.*, Vol. 6, No. 2, Pp. 240–249, 2023.

[2] A. Farazin And S. F. Darghiasi, "Hydroxyapatite-Based Nanocomposite Scaffolds For Bone Regeneration," *Int. J. Appl. Ceram. Technol.*, No. August, 2025.

[3] F. L. Muntean *Et Al.*, "Hydroxyapatite From Mollusk Shells: Characteristics, Production, And Potential Applications In Dentistry," *Dent. J.*, Vol. 12, No. 12, Pp. 1–24, 2024.

[4] M. Trzaskowska, V. Vivcharenko, And A. Przekora, "The Impact Of Hydroxyapatite Sintering Temperature On Its Microstructural, Mechanical, And Biological Properties," *Int. J. Mol. Sci.*, Vol. 24, No. 6, 2023.

[5] D. J. Patty, A. D. Nugraheni, I. D. Ana, And Y. Yusuf, "In Vitro Bioactivity Of 3d Microstructure Hydroxyapatite/Collagen Based-Egg White As An Antibacterial Agent," *J. Biomed. Mater. Res. - Part B Appl. Biomater.*, Vol. 110, No. 6, Pp. 1412–1424, 2022.

[6] R. Patel And A. P. Jain, "Preparation And Characterization Of Levodopa-Selegiline Loaded Chitosan Nanoparticles," *Int. J. Medical, Pharm. Heal. Sci.*, Vol. 1, No. 1, Pp. 34–40, 2024.

[7] S. Rahayu, Masruroh, D. J. D. H. Santjojo, N. Septiani, And R. Wirawan, "Isolation And Characterization Of Chitosan From Nacre Of The Oyster Pearl Shell (*Pinctada Maxima*) As Biopolimer," *J. Phys. Conf. Ser.*, Vol. 2980, No. 1, 2025.

[8] D. W. Kurniawidi *Et Al.*, "Modification Of Chitosan Isolation Method From Pearl Oyster Shell (*Pinctada Maxima* Sp) As A Source Of Natural Polymer," *J. Phys. Conf. Ser.*, Vol. 2866, No. 1, 2024.

[9] G. Alawiyah *Et Al.*, "Synthesis Of Nanochitosan From Oyster Pearl Shell (*Pinctada Maxima*) As Renewable Energy Candidate," *Acta Chim. Asiana*, Vol. 7, No. 2, Pp. 526–533, 2024.

[10] International Organization For Standardization, "Iso 13779-3:2018 - Implants For Surgery — Hydroxyapatite — Part 3: Chemical Analysis And Characterization Of Crystallinity Ratio And Phase Purity," Geneva, 2018

[11] D. Sonin *Et Al.*, "Biological Safety And Biodistribution Of Chitosan Nanoparticles," *Nanomaterials*, Vol. 10, No. 4, Pp. 1–23, 2020.

[12] C. K. Ng *Et Al.*, "Characterization And Sintering Properties Of Hydroxyapatite Bioceramics Synthesized From Clamshell Biowaste," *Iium Eng. J.*, Vol. 23, No. 2, Pp. 228–236, Jul. 2022.

[13] A. Sangmala, P. Naemchanthara, P. Limsuwan, And K. Naemchanthara, "Replacement Of Hydroxyapatite From Chicken Eggshell Waste For Ceramic Properties Improvement," *Int. J. Appl. Ceram. Technol.*, Vol. 18, No. 6, Pp. 2132–2142, Nov. 2021.

[14] K. Niziołek, D. Słota, J. Sadlik, E. Łachut, W. Florkiewicz, And A. Sobczak-Kupiec, "Influence Of Drying Technique On Physicochemical Properties Of Synthetic Hydroxyapatite And Its Potential Use As A Drug Carrier," *Materials (Basel).*, Vol. 16, No. 19, 2023.

[15] S. Yarnpakdee, T. Senphan, S. Karnjanapratum, C. Jaisan, And S. Wangtueai, "Structural Characterization And Antibacterial Activity Of Pearl Oyster (*Pinctada Maxima*) Shell As

Affected By Calcination Temperature," *J. Agric. Food Res.*, Vol. 19, No. April 2024, P. 101551, 2025.

[16] B. Fatima, "Quantitative Analysis By Ir: Determination Of Chitin/Chitosan Dd," *Mod. Spectrosc. Tech. Appl.*, 2020.

[17] A. Kurzyk *Et Al.*, "Calcination And Ion Substitution Improve Physicochemical And Biological Properties Of Nanohydroxyapatite For Bone Tissue Engineering Applications," *Sci. Rep.*, Vol. 13, No. 1, Pp. 1–17, 2023.

[18] F. Fendi, B. Abdullah, S. Suryani, I. Raya, And D. Tahir, "The Use Of Waste Bones Of Rabbitfish (Siganus Sp.) For The Synthesis Of Hydroxyapatite," *Iop Conf. Ser. Earth Environ. Sci.*, Vol. 1230, No. 1, P. 012042, Sep. 2023.

[19] D. J. Patty, A. D. Nugraheni, I. Dewi Ana, And Y. Yusuf, "Mechanical Characteristics And Bioactivity Of Nanocomposite Hydroxyapatite/Collagen Coated Titanium For Bone Tissue Engineering," *Bioengineering*, Vol. 9, No. 12, 2022.

[20] M. Megawati, D. J. Patty, And Y. Yusuf, "Synthesis And Characterization Of Carbonate Hydroxyapatite From *Pinctada Maxima* Shell With Short Aging Time For Bone Biomaterial Candidate," *Eng. Chem.*, Vol. 3, Pp. 13–18, 2023.

[21] N. Bayram, S. Dikmen, And S. Malkoç, "Effect Of Different Calcination Temperatures On Synthesized Hydroxyapatites From Waste Eggshell," *Eskişehir Tech. Univ. J. Sci. Technol. A - Appl. Sci. Eng.*, Vol. 25, No. 4, Pp. 590–601, 2024.

[22] D. J. Patty, A. D. Nugraheni, I. D. Ana, And Y. Yusuf, "In Vitro Bioactivity Of 3d Microstructure Hydroxyapatite/Collagen Based-Egg White As An Antibacterial Agent," *J. Biomed. Mater. Res. Part B Appl. Biomater.*, Vol. 110, No. 6, Pp. 1412–1424, Jun. 2022.

[23] N. A. S. M. Pu'ad, P. Koshy, H. Z. Abdullah, M. I. Idris, And T. C. Lee, "Syntheses Of Hydroxyapatite From Natural Sources," *Heliyon*, Vol. 5, No. 5, Pp. 1–14, 2019.

[24] A. Hosney, S. Ullah, And K. Barčauskaitė, "A Review Of The Chemical Extraction Of Chitosan From Shrimp Wastes And Prediction Of Factors Affecting Chitosan Yield By Using An Artificial Neural Network," *Mar. Drugs*, Vol. 20, No. 11, 2022.

[25] H. Aldila, Asmar, V. A. Fabiani, D. Y. Dalimunthe, And R. Irwanto, "The Effect Of Deproteinization Temperature And Naoh Concentration On Deacetylation Step In Optimizing Extraction Of Chitosan From Shrimp Shells Waste," *Iop Conf. Ser. Earth Environ. Sci.*, Vol. 599, No. 1, 2020.

[26] R. E. Des Bouillons-Gamboa *Et Al.*, "Synthesis Of Chitosan Nanoparticles (Csnp): Effect Of Ch-Ch-Tpp Ratio On Size And Stability Of Nps," *Front. Chem.*, Vol. 12, No. November, Pp. 1–14, 2024.

[27] R. Jha And R. A. Mayanovic, "A Review Of The Preparation, Characterization, And Applications Of Chitosan Nanoparticles In Nanomedicine," *Nanomaterials*, Vol. 13, No. 8, 2023.

[28] M. E. S. Ahmed, M. I. Mohamed, H. Y. Ahmed, M. M. Elaasser, And N. G. Kandile, "Fabrication And Characterization Of Unique Sustain Modified Chitosan Nanoparticles For Biomedical Applications," *Sci. Rep.*, Vol. 14, No. 1, Pp. 1–18, 2024.

[29] E. Alehosseini, H. Shahiri Tabarestani, M. S. Kharazmi, And S. M. Jafari, "Physicochemical, Thermal, And Morphological Properties Of Chitosan Nanoparticles Produced By Ionic Gelation," *Foods*, Vol. 11, No. 23, 2022.